Physica A 466 (2017) 663–671

Contents lists available at ScienceDirect

Physica A

journal homepage: www.elsevier.com/locate/physa

Complex network analysis of brain functional connectivity under a multi-step cognitive task

Shi-Min Cai [a,b], Wei Chen [a,b], Dong-Bai Liu [c], Ming Tang [a,b], Xun Chen [d,*]

[a] Web Sciences Center, School of Computer Science and Engineering, University of Electronic Science and Technology of China, Chengdu 610073, PR China

[b] Big Data Research Center, University of Electronic Science and Technology of China, Chengdu 610073, PR China

[c] Department of Neurology, The Affiliated Jiangyin Hospital of Southeast University of Medical College, Jiangyin 214400, PR China

[d] Department of Biomedical Engineering, Hefei University of Technology, Hefei 230009, PR China

HIGHLIGHTS

- We analyze the functional connectivity of behavioral brain activity.
- The brain organization is a generic small-world and scale-free network.
- The functional connectivity differentiates from the order of behaviors performed.
- The functional connectivity is strongly correlated with activated ROIs.

ARTICLE INFO

Article history:
Received 13 April 2016
Received in revised form 27 July 2016
Available online 5 October 2016

Keywords:
Functional connectivity
Brain network
Behavioral activity
fMRI
Complex network theory

ABSTRACT

Functional brain network has been widely studied to understand the relationship between brain organization and behavior. In this paper, we aim to explore the functional connectivity of brain network under a *multi-step* cognitive task involving consecutive behaviors, and further understand the effect of behaviors on the brain organization. The functional brain networks are constructed based on a high spatial and temporal resolution fMRI dataset and analyzed via complex network based approach. We find that at voxel level the functional brain network shows robust small-worldness and scale-free characteristics, while its assortativity and rich-club organization are slightly restricted to the order of behaviors performed. More interestingly, the functional connectivity of brain network in activated ROIs strongly correlates with behaviors and is obviously restricted to the order of behaviors performed. These empirical results suggest that the brain organization has the generic properties of small-worldness and scale-free characteristics, and its diverse functional connectivity emerging from activated ROIs is strongly driven by these behavioral activities via the plasticity of brain.

© 2016 Elsevier B.V. All rights reserved.

1. Introduction

Human brain, consisting of billions of neurons and synapses, is perhaps the most complex system ever known. Its structural (or anatomic) and functional organization both behave as complicated connectivity in the view of graph and have been widely investigated via complex network theory in the neuroscience community. Plenty of works focus on

* Corresponding author.
E-mail address: xunchen@ece.ubc.ca (X. Chen).

http://dx.doi.org/10.1016/j.physa.2016.09.058
0378-4371/© 2016 Elsevier B.V. All rights reserved.

the topological properties of structural and functional brain networks derived from diffusion MRI, functional MRI (fMRI), electroencephalograph (EEG), magnetoencephalography (MEG), and multielectrode array (MEA) data [1–6]. These networks show both the generic small-worldness [7] and scale-free characteristics [8] independent from the physiological and pathological states [9–13]. And, they also suggest high topological efficiency, robustness, modularity and rich club of hubs [14–21].

It is also well known that a human brain is a physically expensive system to built and run, that is, the adaptive responses (e.g., the capacity for information processing) of a brain network are constrained by its wiring costs [14,15,22–25]. In other words, the macro-scale functional response of human brain emerges from the synergistic dynamics of micro-scale coupled neurons. Thus, the links between the brain structure and function can be suggested by the neurons' dynamic activities. For example, Honey et al. firstly used a computational approach to relate the functional response of *resting-state* brain activity to the underlying structural connectivity and find there are structure–function correlations at multiple temporal scales [26]. Furthermore, they demonstrate that although the resting-state functional connectivity frequently exists between spatially distributed regions without direct structural edges, its strength, persistence and spatial statistics are constrained by whole structural organization [27]. Similar result is also found in Refs. [25,28].

We have known that the structural and functional connectivity are characterized by common features, and the functional connectivity is also correlated with the structural one even when the brain activity evolves in the resting state. However, insofar as we know, how the multi-step behavioral activities affect the emergence of functional connectivity and how its functional features involve with the structural organization have not yet been comprehensively studied by using complex network theory. Herein, complex network based approach is applied to analyze the functional connectivity when the brain activates under a multi-step cognitive task. The functional brain networks are constructed at voxel and ROI (i.e., region of interests, functional area of structure organization) levels from the high spatially and temporally resolved fMIR dataset. We find that at voxel level the functional brain network shows a number of the statistic features, such as small-worldness, scale-free characteristics, assortativity and rich-club organization, which are trivially affected by the order of behaviors performed. More interestingly, at ROIs level, some statistic features of functional brain network are obviously restricted to the order of behaviors performed and correlated with these activated ROIs. These empirical results suggest that the brain organization has some generic properties and the diverse function connectivity emerging from activated ROIs is strongly driven by these human behaviors via the plasticity of brain.

2. Materials and method

2.1. Materials

The benchmark StarPlus fMRI dataset is collected by Just and his colleagues in the $*/+/\$$ experiment at the Center for Cognitive Brain Imaging of Carnegie Mellon University [29–31]. In this cognitive experiment, there are two different sessions for each individual subject. The difference of the two sessions is the distinct order of behaviors performed that involve semantical and symbol stimulus. These two sessions are, respectively, divided into four independent blocks, and each one was composed of a number of trials. More specifically, each trial consisted of cognitive and rest segments. In the cognitive segments of the first session, subjects are presented with a sentence (semantic stimulus) on a screen such as "It is true that the star is below the plus" for 4 s; then the sentence is replaced with a black screen for another 4 s; finally subjects are shown with a picture (symbol stimulus) depicting the geometric arrangement of the symbols $*$ and $+$, and the subjects should quickly judge whether the sentence describes the picture correctly or not by pressing a button with the choice "yes" or "no". Once the judgment is made or lasted more than 4 s, the picture would be removed from the screen. Before repeating the next trial, there is a 15-s rest segment. The second session has the similar procedure by simply switching the order of presenting sentence and the picture.

The fMRI images were collected every 0.5 s with the resolution $64 \times 64 \times 8$. Thus, there are around 54 images (27 s) available for each trial. A total of twenty trials are implemented for each subject in each session. We denote the two sessions as P (a picture presented before a sentence) and S (a sentence shown before a picture), respectively. For each session, the block was made up by several (4 or 8) continuous trials and thus contained rest segments between adjacent trials.

Additionally, the cognitive experiments engaged several functional areas of cerebral cortex (i.e., structural organization of brain), such as visual area for the sentence/symbol reading (occipital lobe), spatial visualization (inferior parietal sulcus, e.g. LIPS and RIPS) and recognizing (inferior temporal, e.g. LIT, RIT, LT and RT), Broca area for language processing (left inferior frontal gyrus, e.g. LIFG), Wernicke area for semantic analyzing (middle and superior temporal gyrus, angular gyrus, e.g. LTRIA and RTRIA), motor area for the button pressing (supplementary motor area, e.g., SMA, LDLPFC and RDLPFC), etc. Therefore, the voxels (i.e., 3-dimension pixels) of fMRI images were anatomically allocated into 25 ROIs. Based on that, the functional connectivity of brain network constructed from these fMRI time series can be investigated at both small (voxel) and large (ROI) levels.

2.2. Functional brain network construction

The functional brain networks are extracted from the fMRI time series. At time t, the fMRI images of brain activity are measured by a group of voxels. Thus, the voxel time series $T(t, v)$ characterize the functional changes of cerebra cortex,

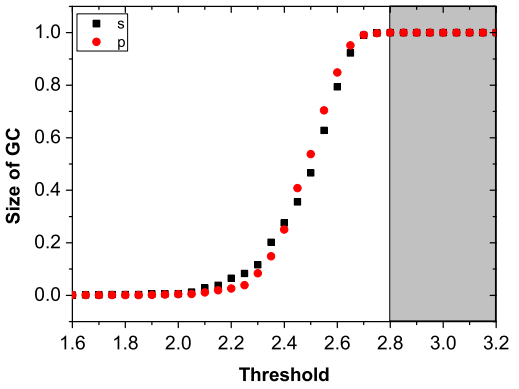

Fig. 1. (Color online) The relationship between the threshold and the size of giant component (GC). The size of GC is equal to 1 in gray area, whose left edge of the gray area shows the point of percolation phase transition that is fixed as the threshold of binarization.

and their correlations imply the functional connectivity of areas of cerebra cortex. Taking these into consideration, it is natural to define the nodes of functional brain network by these voxels, and associate their links with the correlations. To encapsulate the temporal and spatial correlations, a synthetic measure is proposed here by coupling the Pearson correlation and Euclidean distance. The calculation procedure will be described as follows. For a block x in session P, we first compute the Euclidean distance between each pair of the nodes, v_i and v_j:

$$E_x(v_i, v_j) = \sqrt{\sum_{k=1}^{n} (T_x(t_k, v_i) - T_x(t_k, v_j))^2}, \tag{1}$$

where n denotes the length of voxel time series. Hence, we get

$$E_p(v_i, v_j) = \langle E_x(v_i, v_j) \rangle \quad x \in P, \tag{2}$$

where $\langle \cdot \rangle$ represents the mathematical expectation. $E_p(v_i, v_j)$ determines the Euclidean distance between nodes v_i and v_j. The larger Euclidean distance suggests the weaker spatial correlation.

On the other hand, the Pearson correlation between each pair of nodes, v_i and v_j, is computed as

$$R_x(v_i, v_j) = \frac{\langle T_x(t, v_i) T_x(t, v_j) \rangle - \langle T_x(t, v_i) \rangle \langle T_x(t, v_j) \rangle}{\sigma(T_x(v_i)) \sigma(T_x(v_j))}, \tag{3}$$

where $\sigma^2(T_x(v)) = \langle T_x(t, v)^2 \rangle - \langle T_x(t, v) \rangle^2$. And, we also get

$$R_p(v_i, v_j) = \langle R_x(v_i, v_j) \rangle \quad x \in P. \tag{4}$$

To characterize the Pearson correlation by a distance metric (termed as correlation distance), an alternative approach satisfying the three axioms [32] is

$$R'_p(v_i, v_j) = \sqrt{2(1 - R_p(v_i, v_j))}. \tag{5}$$

As $R_p(v_i, v_j)$ ranges from $[-1, 1]$, $R'_p(v_i, v_j)$ varies from $[0, 2]$. It is emphasized that the smaller $R_p(v_i, v_j)$, indicating weaker temporal correlation, corresponds to the larger $R'_p(v_i, v_j)$. Thus, the correlation distance is analogous to the Euclidean distance.

Finally, the synthetic measure of the correlation between each pair of nodes, v_i and v_j, is defined by the linear combination of correlation distance and Euclidean distance:

$$D_p(v_i, v_j) = (1 - \alpha) R'_p(v_i, v_j) + \alpha E_p(v_i, v_j). \tag{6}$$

The coupling coefficient α makes $E_p(v_i, v_j)$ and $R'_p(v_i, v_j)$ at the roughly same range and guarantees the balance between these two types of distances since their probability distributions have a similar shape [33]. For the session S, $D_s(v_i, v_j)$ can be obtained in the same way.

Although the synthetically measured matrix is able to characterize a weighted functional brain network, we binarize it into adjacent one A by choosing a proper threshold to simply and accurately quantify the functional connectivity of brain network. The threshold is fixed by a percolation-based method that determines the size of giant component (GC), i.e., the largest connected subnetwork. Fig. 1 shows that the size of GC changes as a function of threshold, suggesting that it gradually converges to 1 with increasing threshold. And the point of percolation phase transition can be found at the left edge of the gray area in Fig. 1, which is properly fixed as the threshold of binarization, $d_c = 2.8$. Then, we assume that two nodes are functionally connected (i.e., $a_{i,j} = 1$, $a_{i,j} \in A$) if their distance $D(v_i, v_j)$ does not exceed the threshold value d_c. Finally, a adjacent matrix is obtained to represent the functional brain network.

2.3. Metrics

Once the functional brain network is extracted, complex network theory, as a common and effective method, is utilized to analyze the functional connectivity. The measurements of topological structure are divided into voxel and ROI levels. To keep our description as self-contained as possible, a amount of important metrics should be reviewed briefly.

Degree k_i of a node i is the number of edges incident with the node, and is defined as

$$k_i = \sum_{j=1}^{N} a_{ij}, \tag{7}$$

where a_{ij} is an element of A and N is the total number of nodes. $\langle k \rangle$ thus denotes the average degree (AD) of the whole network. The most basic topological feature of a network is the degree distribution P_k, involved with the probability that a node is chosen randomly.

Clustering coefficient (CC) c_i of a node i is defined as the ratio of the number of edges between its neighbors (E_i) with respect to the total one as

$$c_i = \frac{2E_i}{k_i(k_i - 1)}. \tag{8}$$

The CC of whole network, C, is the average value of all c_i.

Path length (PL) d_{ij} between two vertices i and j is the number of edges through the shortest path. The average path length L is calculated by averaging the path lengths of each pair of nodes as

$$L = \frac{1}{\frac{1}{2}N(N+1)} \sum_{i \geq j} d_{ij}. \tag{9}$$

Assortativity coefficient (AC) r is adopted to depict mixing pattern, and is defined as

$$r = \frac{\sum_{jk} jk(e_{jk} - q_j q_k)}{\sigma_q^2} \tag{10}$$

where $q_k = \frac{(k+1)P_{k+1}}{\sum_j jP_j}$ denotes the normalized distribution of the remaining degree, e_{jk} is defined as the joint probability distribution of the remaining degrees, and $\sigma_q^2 = \sum_k k^2 q_k - [\sum_k k q_k]^2$ is the variance of the distribution q_k [34]. For assortative mixing $r > 0$, it suggests that nodes prefer to connect with their similar one, while for disassortative mixing $r < 0$, it shows that the connections are more likely to occur between dissimilar nodes [35].

The importance of a node in a network is usually characterized by a series of centrality indices. Besides node's degree, coreness and betweenness are often employed. The coreness of a node i is k if the node i belongs to k-core but does not exist in $(k+1)$-core, where k-core is the connected components of subgraph formed by repeatedly deleting all nodes with degree less than k [36]. Meanwhile, betweenness of a node i is defined as the sum of the shortest paths via node i [37],

$$BC_i = \sum_{s,t \in N, s \neq i \neq t} d_{st}^i. \tag{11}$$

Average neighbor degree k_{nn}^i of a node i is used to describe degree–degree correlation that associates with mixing pattern, and is defined as

$$k_{nn}^i = \sum_{j \in N} \frac{a_{i,j} k_j}{k_i}. \tag{12}$$

The rich-club organization characterizes larger degree nodes' connectivity. The rich-club coefficient $\Phi(r/N)$ denotes the ratio of the number of existence edges m with respect to the maximum number of possible edges $r(r-1)/2$ among those first r nodes with the largest degree [38,39], which is described as

$$\Phi(r/N) = \frac{2m}{r(r-1)}. \tag{13}$$

3. Results and discussion

3.1. Analysis of functional connectivity at voxel level

Herein, the functional brain networks constructed from fMRI time series at two sessions, P and S, are concurrently analyzed to investigate the effect of order of behaviors performed on functional connectivity. Firstly, as shown in Table 1, the statistical features of two functional brain networks are represented by generally characteristic parameters, C,

Table 1
The average of characteristic parameters for two functional brain networks.

	N	C	$\langle k\rangle$	L	r
P	4949	0.4220	129.2831	2.7340	0.1318
S	4949	0.4202	127.6193	2.7174	0.0545

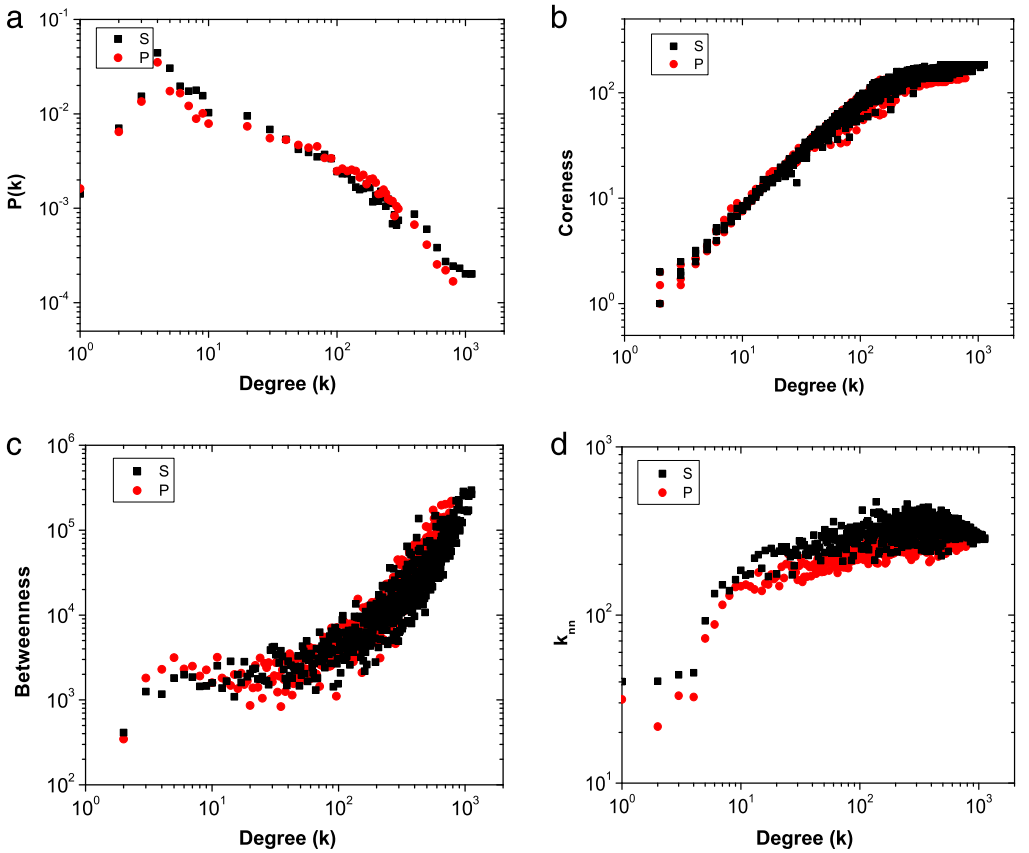

Fig. 2. (Color online) (a) Degree distributions at a log–log scale for two functional brain networks. Both of them have a power-law tail that suggests the scale-free characteristics. (b) Coreness as a function of degree k. The relation between coreness and degree for two functional brain networks approximately obeys a power-law increasing trend when k ranges from 10^0 to 10^2, but remains unchanged when k exceeds 10^2. (c) Betweenness as a function of degree k. The relation between betweenness and degree for two functional brain networks approximately keeps stable when degree is less than 10^2, but obeys a power-law increasing trend when k exceeds 10^2. Note that both the coreness and betweenness centrality behave trivially different between P and S. (d) Degree–degree correlation measured through k_{nn}, a function of k. The positive correlation and the roughly different increasing slopes of relationship between k_{nn} and k confirm the result obtained from assortativity coefficient.

$\langle k\rangle$, L and r. Both of them are closely connected and represented by large $\langle k\rangle$, and the large C and small L show the robust small-worldness. However, although $r > 0$ denotes assortative mixing of functional brain networks, its strength differentiates from each other. These results straightly suggest that the small-worldness independent from ordering of behaviors performed is the generic property of brain organization, yet to some extent the topological structures of functional brain networks are also restricted to transient changes of behaviors.

Then, we analyze topological properties involving with nodes' degrees in detail. The degree distribution is a basic measurement. It is presented at a log–log scale (using logarithmic bin) for two functional brain networks, respectively. As shown in Fig. 2(a), it can be seen that the degree distributions are both approximately close to a power law across multiple scales, which suggests the scale-free characteristics. Moreover, the scale-free topological structure implies that there exists hub-like nodes connecting with most of other ones and these nodes are distributed into activated (or task-related) ROIs (see in Fig. 6).

The scale-free characteristics show a heterogeneous nodes' connectivity of functional brain network. Thus, these nodes have different importance in the connectivity of functional brain network. Here, we employ the coreness and betweenness to quantify node's importance, and mainly investigate that they have a relation with degree. More concretely, the coreness indicates the depth of node in functional brain network. Even if a node has a very high degree, its coreness may be very small. Like a star network with N nodes, the center node has a degree $N - 1$ but its coreness is 0. We compute each node's

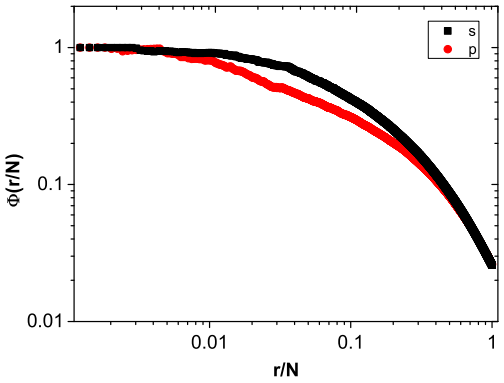

Fig. 3. (Color online) Rich-club coefficient at a double logarithmic scale for two functional brain networks. It suggests that a few of larger degree nodes tend to densely connect with each other and form a stable rich club, yet the nodes with median-scale degrees have different connectivity between *P* and *S*.

coreness according to Ref. [36] and plot them as a function of degree k, as shown in Fig. 2(b). It can be found that at these scales from 10^0 to 10^2 most of nodes' coreness linearly increases with k, yet the nodes with degree larger than 10^2 have approximately similar coreness independent from k and construct the nucleus of functional brain network. Nevertheless, the relation between coreness and degree is trivially different between P and S.

And, the node's betweenness, describing its ability to control the information transitivity based on shortest path routing, is also computed according to Eq. (11). And, the betweenness as a function of k is shown in Fig. 2(c). We can see that the values of betweenness are similar for these nodes with degrees less than 10^2, then approximately increase according to a power law. Similarly, the relation between betweenness and degree is trivially different between P and S. However, combining with the results in Fig. 2(c) and (b), we can deduce that the nucleus of a functional brain network (e.g., these large degree nodes with $k > 10^2$) controls and undertakes the information transitivity of functional response, and the functional brain networks are easily affected by behavioral activities.

Furthermore, the degree–degree correlation measured through k_{nn} as a function of k reflects a potential mixing pattern. The assortative mixing is denoted by the positive correlation that k_{nn} increases with k, while the disassortative mixing is described by the negative correlation that k_{nn} decreases with k. Fig. 2(d) shows the relationship between k_{nn} and k for two functional brain networks. Obviously, both of them are assortative mixing because k_{nn} positively increase with k; however, the increasing slopes are roughly different. These results also correspond to assortativity coefficients in Table 1. Note that the macroscopically quantitative difference of assortative mixing for two functional brain networks may arise from the extent of activation in visual and semantic areas. Thus, the order of behaviors performed does not affect the assortative mixing of functional brain networks, but trivially alters the assortativity coefficients.

The rich-club organization indicates that there exist a few larger degree nodes in network, and these nodes tend to densely connect with each other to constitute "rich club". In Refs. [19,40,41], they have demonstrated that a small set of functional areas (i.e., nodes in functional brain network) are highly connected to form a dense rich club that play a central role in global information integration. That is, the existence of rich club organization in functional brain network is due to the functional response of human brain. Herein, the rich-club coefficient is quantitatively shown in Fig. 3. We can see that approximately 1% nodes are almost completely connected regardless of the order of behaviors performed; however, these nodes with median-scale degrees (e.g., $r/N \in [0.01, 0.4]$) have different connectivity in restriction to the order of behaviors performed. Thus, these results suggest that these nodes in rich club enable efficient information communication, while those nodes with median-scale degrees play a non-trivial role in local information integration and correspond to some functional areas related to behaviors. Furthermore, although the average degrees of two functional brain networks are almost equal, the functional brain network P has some larger degree nodes ($>10^3$) than the functional brain network S (see in Fig. 2(a)). It leads to the difference of degree heterogeneity between P and S. Thus, the difference of functional connectivity among the nodes with median-scale degrees may arise from the degree heterogeneity.

3.2. Analysis of functional connectivity at ROI level

Since the voxels have been distributed into 25 anatomically defined ROIs as mentioned above, it is interesting to probe the functional connectivity of brain network at ROI level. Specifically speaking, we allocate the voxels (i.e., nodes) into 25 ROIs through ignoring external edges between ROIs, and obtain 25 isolated functional subnetworks. Note that there are 22 ROIs symmetrically distributed into left and right hemispheres. Fig. 4 shows that the sizes of subnetworks are heterogeneous, of which the maximum is 498 and the minimum is 13, and approximately symmetrical for left and right hemispheres (except of ROI 9 and 20). Note that the heterogeneous subnetworks corresponding to ROIs arise from the difference of ROI's anatomic structure. The horizontal axis labels 25 different ROIs, of which the order is consistent with the following plots (see in Fig. 4).

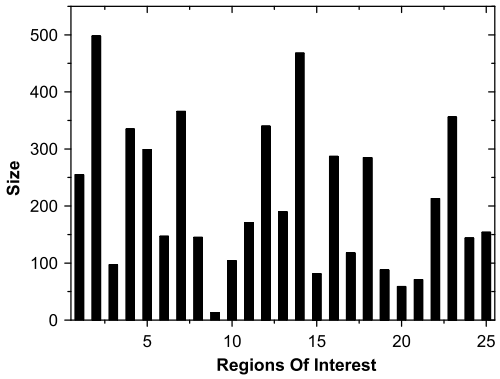

Fig. 4. Size of subnetworks at ROI level. These subnetworks show the heterogeneous size and connectivity density. The horizontal axis from 1 to 25 represents the ROIs, "CALC","LDLPFC", "LFEF", "LIFG", "LIPL", "LIPS", "LIT", "LOPER", "LPPREC", "LSGA", "LSPL", "LT", "LTRIA", "RDLPFC", "RFEF", "RIPL", "RIPS", "RIT", "ROPER", "RPPREC", "RSGA", "RSPL", "RT", "RTRIA", and "SMA". .

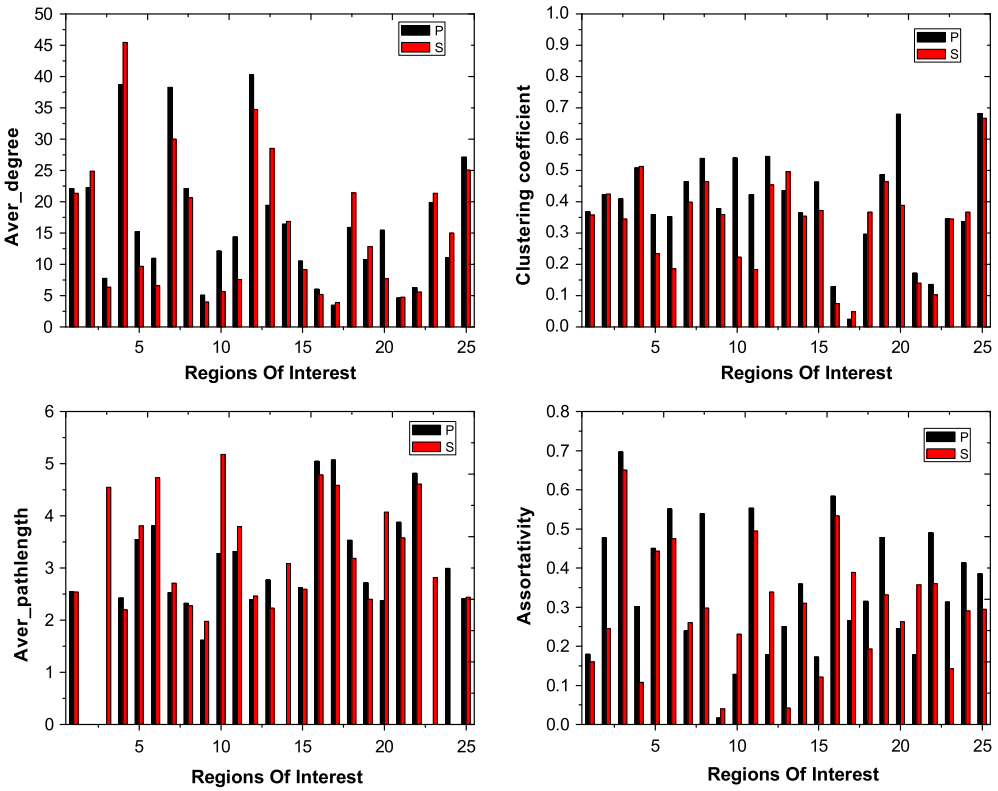

Fig. 5. (Color online) The statistical average values of four measurements, AD, CC, PL and AC, restricted to 25 ROIs (or subnetworks). Note that the PL is equal to 0 due to incompletely connected subnetworks. The heterogeneous values of four measurements suggest that the functional connectivity strongly correlates with ROIs, and is driven by behaviors.

For these 25 subnetworks, we also focus on the measurements including AD, CC, PL, and assortativity. The statistical average values of four measurements restricted to *P* and *S* are shown in Fig. 5, which suggests that the functional connectivity is different between each pair of subnetworks, especially in those corresponding to activated ROIs. More specifically, in the Fig. 5(a), the AD of subnetworks corresponding to the activated ROIs 4, 7 (or 18), 12 (or 23), 25 is obviously larger than others, and behave significantly different between *P* and *S* except activated ROI 25. It suggests that the connectivity of subnetworks strongly associates with specific functional areas of cerebral cortex, and is obviously restricted to the order of behaviors performed. In Fig. 5(b) and (c), they show the larger CC and lower PL for all subnetworks regardless of behaviors, which suggests the generic property of small-worldness. Due to the subnetworks are not guaranteed to completely connect, the PL misses in some of them. Moreover, in Fig. 5(d), the assortativity suggests assortative mixing remaining in subnetworks although their values are heterogeneous.

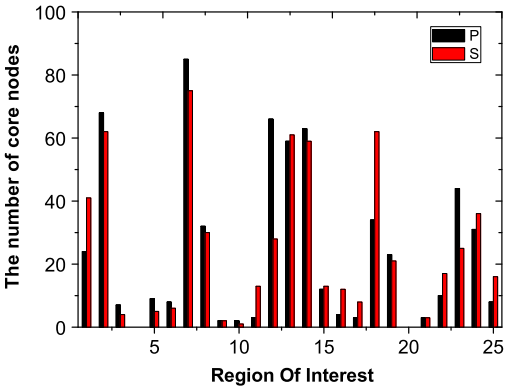

Fig. 6. (Color online) The most important 600 core nodes in terms of coreness are distributed into 25 ROIs. We can find that these activated ROIs 2, 7, 12, 13, 14, 18, 23, 24 strongly associated with cognitive function obviously include more core-like nodes, and some of them behave significant different between *P* and *S*.

Nodes with high coreness are more important than those with low coreness as mentioned above. We choose the most important 600 nodes in terms of the coreness and count how many vertices in each ROI, to unveil which ROIs the nodes are mostly distributed in and whether the distribution has any differences with respect to diverse cognitive states. Fig. 6 shows the number of core nodes in each ROI restricted to *P* and *S*. It can be found that the ROI 7 (i.e., LIT) contains maximum nodes, and most of them are distributed in temporal area (such as ROIs 12 (LT), 13 (LTRIA), 18 (RIT), 23 (RT), and 24 (RTRIA)) and central area (such as ROIs 2 ((LDLPFC) and 14 (RDLPFC))). Furthermore, the biggest difference for *S*and *P* is also behaved in these ROIs 7, 12, 18, and 23. This suggests that the brain temporal lobes play a key role in cognition, and when a subject judge whether a sentence described a picture correctly, the subject may take more attention to the second stimulus, one explanation is that human always has a deeper impression to the most recent stimulus. As is well-known in literature, the temporal lobes are involved in the retention of visual memories, processing sensory input, comprehending language, storing new memories, emotion, and senior visual function (such as object recognition) [42]. Thus, the empirical results are consistent with previous findings.

4. Conclusion

The emphasis of this work unveils the association between brain organization and behavioral activities. We systematically and comparatively analyze the function connectivity of brain network via complex network theory when an individual performs a consecutively cognitive task involving diverse behaviors. At voxel level, the functional brain network shows the generic properties of small-worldness and scale-free characteristics, while its assortativity and rich club organization are slightly restricted to the order of behaviors performed. Furthermore, we divide the functional brain network into 25 subnetworks corresponding to intra structural organization of ROIs, and find that these activated ROIs associated with cognitive task obviously have larger AD and more core-like nodes. Especially, these subnetworks corresponding to activated ROIs show that their functional connectivities are restricted to the order of behaviors performed. Thus, these empirical results suggest that the brain organization represented by the functional connectivity are strongly driven by human behavioral activity (or cognitive task) via the plasticity of brain.

Acknowledgments

This work is partially supported by the National Natural Science Foundation of China (Grant Nos. 61004002, 11575041, 61501164, 81571760 and 61673086) and the Fundamental Research Funds of the Central Universities (Grant No. ZYGX2015J153).

References

[1] E.T. Bullmore, O. Sporns, Nat. Rev. Neurosci. 10 (2009) 186.
[2] O. Sporns, NeuroImage 62 (2012) 881.
[3] E.T. Bullmore, O. Sporns, Nat. Rev. Neurosci. 13 (2012) 336.
[4] F. De Vico Fallani, J. Richiardi, M. Chaavez, S. Archard, Philos. Trans. R. Soc. B 369 (2014) 20130521.
[5] J. Zhang, K.M. Kendrick, G. Lu, J. Feng, Cereb. Coretex 25 (10) (2014) 3475.
[6] H. Cui, et al., Hum. Brain Mapp. 37 (2016) 1459.
[7] D.J. Watts, S.H. Strogatz, Nature 393 (1998) 440.
[8] A.L. Barabási, R. Albert, Science 286 (1999) 509.
[9] V.M. Eguiluz, D.R. Chialvo, G.A. Cecchi, M. Baliki, A.V. Apkarian, Phys. Rev. Lett. 94 (1) (2005) 018102.
[10] Y. He, Z.J. Chen, A.C. Evans, Cereb. Coretex 17 (2007) 2407.
[11] M.P. van den Heuvel, C.J. Stam, M. Boersma, H.E. Hulshoff Pol, NeuroImage 43 (2008) 528.

[12] D.S. Bassett, E.T. Bullmore, Curr. Opin. Neurol. 22 (2009) 340.
[13] C.J. Stam, E.C.W. van Straaten, Clin. Neruophysiol. 123 (2012) 1067.
[14] M. Kasier, C.C. Hilgetag, PLoS Comput. Biol. 2 (2006) e95.
[15] R. Achard, E.T. Bullmore, PLoS Comput. Biol. 3 (2007) e1.
[16] D. Meunier, R. Lambiotte, A. Fornito, K.D. Ersche, E.T. Bullmore, Front. Neuroinf. 3 (2009) 37.
[17] P. Hagmann, L. Cammoun, X. Gigandet, R. Meuli, C.J. Honey, V.J. Wedeen, O. Sporns, PloS Biol. 6 (2008) e159.
[18] M. Chavez, M. Valencia, V. Navarro, V. Latora, J. Martinerie, Phys. Rev. Lett. 104 (2010) 118701.
[19] M.P. van den Heuvel, O. Sporns, J. Neurosci. 31 (2011) 15775.
[20] Z. Zhuo, S.M. Cai, Z.Q. Fu, J. Zhang, Phys. Rev. E 84 (2011) 031923.
[21] O. Sporns, R.F. Betzel, Ann. Rev. Psychol. 67 (19) (2016) 19.
[22] M.P. van den Heuvel, C.J. Stam, R. Kahn, H.E. Hulshoff Pol, J. Neurosci. 29 (2009) 7619.
[23] L.K. Galos, H.A. Makse, M. Sigman, Proc. Natl. Acad. Sci. USA 109 (2012) 2825.
[24] A. Zalesky, A. Fornito, L. Cocchi, L.L. Gollo, M. Breakspear, Proc. Natl. Acad. Sci. 111 (28) (2014) 10341.
[25] M.W. Cole, D.S. Bassett, J.D. Power, T.S. Braver, S.E. Petersen, Neuron 83 (2014) 238.
[26] C.J. Honey, R. Kötter, M. Breakspear, O. Sporns, Proc. Natl. Acad. Sci. 104 (24) (2007) 10240.
[27] C.J. Honey, O. Sprons, L. Cammoun, X. Gigandet, J.P. Thiran, R. Meuli, P. Hagmann, Proc. Natl. Acad. Sci. 106 (6) (2009) 2035.
[28] M.W. Cole, T. Ito, T.S. Braver, Cereb. Coretex 26 (6) (2016) 2497.
[29] P.A. Carpenter, M.A. Just, T.A. Keller, W.F. Eddy, K.R. Thuborn, NeuroImage 10 (1999) 216.
[30] X. Wang, R. Hutchinson, T. Mitchell, Training fMRI Classifiers to Detect Cognitive States across Multiple Human Subjects, in: Proceedings of NIPS'03.
[31] T.M. Mitchell, R. Hutchinson, R.S. Niculescu, F. pereira, X. Wang, M. Just, S. Newman, Mach. Lern. 57 (2004) 145.
[32] S.M. Cai, Y.B. Zhou, T. Zhou, P.L. Zhou, Internat. J. Modern Phys. C 21 (03) (2010) 433.
[33] L. Hong, S.M. Cai, J. Zhang, Z. Zhuo, Z.Q. Fu, P.L. Zhou, Chaos 22 (2012) 033128.
[34] M.E.J. Newman, Phys. Rev. Lett. 89 (20) (2002) 208701.
[35] M.E.J. Newman, Phys. Rev. E 67 (2) (2003) 026126.
[36] M. Gaertler, M. Patrignani, Dynamic analysis of the autonomous system graph, in: Proceedings of International Workshop on Inter-domain Performance and Simulation, IPS 2004, Budapest, Hungary, 2004, pp.13–24.
[37] P. Mahadevan, D. Krioukov, M. Fomenkov, B. Huffaker, X. Dimitropoulos, K. Claffy, A. Vahdat, arXiv:cs/0508033.
[38] S. Zhou, R.J. Mondragón, IEEE Commun. Lett. 8 (3) (2004) 180.
[39] S. Zhou, R.J. Mondragón, Phys. Rev. E 70 (6) (2004) 066108.
[40] L. Harriger, M.P. van den Heuvel, O. Sporns, PLoS One 7 (9) (2012) 446497.
[41] G. Collin, O. Sporns, R.C.W. Mandl, M.P. van den Heuvel, Cereb. Cortex 2 (9) (2014) 2258.
[42] E.E. Smith, S.M. Kosslyn, Cognitive Psychology: Mind and Brain, Prentice Hall, New Jersey, 2006.